Retinal configuration of *p*pR intermediates revealed by photo-irradiation solid-state NMR and DFT

Y. Makino[1], I. Kawamura[1,*], T. Okitsu[2], A. Wada[2], N. Kamo[3], Y. Sudo[4], K. Ueda[1*], A. Naito[1*]

Running title: retinal configuration of *p*pR intermediates

KEYWORDS:

Retinal, *Pharaonis* phoborhodpsin, *in-situ* photo-irradiation solid-state NMR

ABSTRACTS

Pharanois phoborhodopsin (*p*pR) from *Natronomonas pharaonis* is a transmembrane photoreceptor protein involved in negative phototaxis. Structural changes in *p*pR triggered by the photoisomerization of retinal chromophore are transmitted to its cognate transducer protein (*p*HtrII) during a cyclic photo-reaction pathway through several photointermediates called the photo-cycle. It is important to understand the detailed configurational changes of retinal during the photo-cycle. We previously observed one of the photointermediates (M-intermediates) by *in-situ* photo-irradiation solid-state NMR experiments (Y. Tomonaga et al., Biophys. J., **2011**, 101, L50-L52). In this study, we further observed the ^{13}C NMR signals of late photointermediates such as O- and N'-intermediates by illuminating with green light. Under near-UV light irradiation of the M-intermediates, ^{13}C NMR signals of 14- and 20-^{13}C-labeled retinal in the O-intermediate appeared at 115.4 and 16.4 ppm and were assigned to the 13-*trans*, 15-*syn* configuration. The signals due to the N'-intermediate appeared at 115.4 and 23.9 ppm and were in as an equilibrium state with the O-intermediate during thermal decay of the M-intermediates at -60°C. Thus, photo-irradiation NMR studies revealed the photoreaction pathways from the M- to O-intermediates and the equilibrium state between the N'- and O-intermediate. Further,

we evaluated the detailed retinal configurations in the O- and N'-intermediates by performing a DFT chemical shift calculation. The results showed that the N'-intermediate has a 63° twisted retinal state due to the 13-*cis* configuration. The retinal configurations of the O- and N'-intermediates were determined to be 13-*trans*, 15-*syn* and 13-*cis*, respectively, based on the chemical shift values of [20-^{13}C] and [14-^{13}C] retinal obtained by photo-irradiation solid-state NMR and DFT calculation.

INTRODUCTION

Pharaonis phoborhodopsin (*p*pR), also called as sensory rhodopsin II (SRII), is a membrane protein isolated from the halophilic and alkaliphilic archaeon *Natronomonas pharaonis*, which consists of seven-transmembrane α-helices with a vitamin-A aldehyde retinal as a chromophore (1). The all-*trans* retinal is predominantly incorporated into the apoprotein of *p*pR. The *p*pR functions as a photo receptor protein by forming a 2:2 complex with the cognate two-helix transducer protein *p*HtrII to transmit the photo-signal into the cytoplasm (2–5). The *p*pR/*p*HtrII complex involves in a negative phototaxis through a cyclic photo-reaction pathway called the photo-cycle. *p*pR has an absorbance maximum at 498 nm in the ground (G) state under dark conditions as the initial state. Light absorption transforms *p*pR from the ground state (ppR$_G$) to a K(540 nm)-intermediate with an absorbance maximum of 540 nm. This transformation is initiated by *trans*/*cis* photoisomerization of the retinal. The photo-cycle is followed by several intermediates, such as L(498 nm)-, M(390 nm)-, and O(560 nm)-, undergoing thermal relaxation processes. Finally, the O-intermediate thermally returns to the ppR$_G$ state (6).

The K-intermediate has a half-life of approximately 1 μs and its retinal is in the 13-*cis*, 15-*anti* configuration. Transformation of the K-intermediate provides the

L-intermediate, which has half-life of approximately 30 μs and a 13-*cis*, 15-*anti* retinal configuration. Subsequently, a proton is removed from the Schiff base (SB) of the L-intermediate, resulting in transformation to the M-intermediate, which has a long half-life of approximately 1.7 s. The M-intermediate has a 13-*cis*, 15-*anti* retinal configuration with a deprotonated SB (DPSB). Upon reprotonation, the M-intermediate transforms into the O-intermediate with a protonated SB (PSB), which has a half-life of approximately 770 ms and a 13-*trans*, 13-*syn* retinal configuration (4–7). The M- and O-intermediates have long half-lives as compared with the K- and L-intermediates and thus they are known as late-active intermediates.

Important signal transduction processes such as changes in protein structure are induced at the late step in the photo-cycle. These changes likely include the formation of two specific hydrogen bonds, one between $Tyr199^{ppR}$ and $Asn74^{pHtrII}$, and one between $Thr189^{ppR}$ and $Glu43^{pHtrII}$/$Ser62^{pHtrII}$, as observed in the crystal structure of the *p*pR/*p*HtrII complex (8). Thr204 is another important residue in *p*pR, and plays a role in color tuning and in the photo-cycle kinetics of *p*pR (9). Further observations have shown that Thr204 is indispensable for the negative phototaxis function of the complex (10). There is steric hindrance in the K-intermediate between C_{14}-H of retinal and Thr204 (11). At the same time, a specific hydrogen bonding alteration occurs between

Thr204 and Tyr174 in a *p*HtrII-dependent manner (10). Helix movement in *p*pR and outward tilting of helix F during the photo-cycle have been suggested by various groups (12–14) and are believed to be essential steps for the activation of *p*HtrII. However, no helix tilting was observed in the crystal structure of the M-intermediate of the *p*pR/*p*HtrII complex (15). Followed by the tilting of F-helix in *p*pR, TM2 in *p*HtrII rotates, transferring the signal to the phosphorylation cascade to initiate rotation of the bacterial flagellar motor, resulting in negative phototaxis.

The photo-cycle as described above depends on the photo-isomerization of retinal. The retinal chromophore in *p*pR forms a covalent bond with a perfectly conserved Lys residue (Lys205) bonded to a Schiff base. Animal rhodopsin (type II rhodopsin) photobleaches, whereas microbial rhodopsin (type I rhodopsin) retains the retinal through the photo-cycle. Therefore, continuous irradiation of *p*pR with green light results in repeated photo-cycles without photo-breaching and the photo-intermediates can be trapped in stationary state using type I rhodopsins such as *p*pR (1, 5, 16).

Photo-irradiation solid-state NMR spectroscopy has been used to reveal the photo-activated intermediates of retinal membrane proteins. For example, the photo-activated intermediates has been characterized by ^{13}C NMR studies of [^{13}C]

retinal and ^{15}N NMR studies of [ζ-^{15}N]Lys of bacteriorhodopsin (bR) (17–20). The light-adapted state and the M- and N-intermediates of bR have been investigated using photo-irradiation solid-state NMR spectroscopy (18, 19). The early M-intermediate, M_0, and late M-intermediate, M_n, in the bR photo-cycle have been characterized by *in-situ* photo-irradiation solid-state NMR spectrometry (21–23). The combination of NMR spectroscopy with dynamic nuclear polarization (DNP) method revealed the heterogeneity of dark-adapted bR and distortion in K-intermediate, and four discrete L-intermediates were detected (24, 25). In addition to bR, the photoactive site of channel rhodopsin-2 was revealed (26). Thus, we have developed *in-situ* photo-irradiation solid-state NMR apparatus that allows irradiation of the sample with extremely high efficiency and enables observation of the photo-intermediates and photoreaction processes of photoreceptor membrane proteins (27–34).

We previously trapped several photo-intermediates in the photo stationary state using *in-situ* photo-irradiation solid-state NMR and observed the M-intermediates of *p*pR under green light irradiation (28). Continuous irradiation of *p*pR with green light resulted in the accumulation of late-active intermediates such as multiple M-intermediates (M1, M2 and M3) because of their long life times as compared with the early photo–intermediates such as the K- and L-intermediates. Generally, the

half-life of the late intermediates of sensory-type rhodopsin is much longer than that of ion pump-type rhodopsins such as bR (5). It is reasonable that the longer life time of the photo-intermediates in sensory rhodopsins is accompanied by dynamic conformational changes to allow signal transmission to the transducer protein and signal amplification during the photo-cycle, while the fast photocycle is advantageous to transport the ion during the photocycle of ion pump-type rhodopsins.

In this study, we focus on observing the late photo-intermediates after the M-intermediates by performing using *in-situ* photo-irradiation solid-sate NMR equipped with two LED light sources, one each at 520 nm and 365 nm. We previously showed that the ^{13}C NMR signal from [20-^{13}C] retinal responds sensitively to changes in the 13C=14C configuration in retinal. Similarly, ^{13}C NMR signal from [14-^{13}C] retinal should be sensitive to changes of 15C=Nζ configuration in retinal. Here, we specifically detected the ^{13}C NMR signal from [14, 20-^{13}C] labeled retinal in ppR. Based on the chemical shift values for [20-^{13}C] and [14-^{13}C] retinal in the late-active intermediates, and the results of DFT calculations, we discuss the detailed configurations of these intermediates.

MATERIALS AND METHODS

Sample preparation

[14, 20-^{13}C]-Labeled-retinal-*p*pR with a His-tag (6xHis) at the C-terminal was over-expressed in *Escherichia coli* BL21(DE3) strain in LB medium by induction with 1 mM isopropyl-1-thio-β-D-galactoside (IPTG) and 10 μM [14, 20-^{13}C]-labeled-all-*trans*-retinal. Protein expression was performed at 25°C for 15 hrs. To purify the sample, the cells were lysed by ultra-sonication, then the proteins were solubilized using n-dodecyl-β-D-maltoside (DDM) and purified with Ni-NTA (QIAGEN, Hilden, Germany) as previously described (28, 35, 36). *p*HtrII(1-159) was also prepared by the same method as described previously (28). After purification, *p*pR was mixed with *p*HtrII at a 1:1 molar ratio by electrophoresis and by monitoring UV-vis absorption and thermal stability (37) of the *p*pR/*p*HtrII complex. The complex was reconstituted into membrane, in DDM micelles incorporating a lipid film of L-α-egg-phosphatidylcholine (Egg-PC) (*p*pR:Egg-PC molar ratio of 1:30), then DDM was removed by using Bio-Beads (Bio-RAD, Hercules, CA). The reconstituted samples were suspended in 5 mM 2-[4-(2-hydroxyethyl-1-piperazinyl) ethanesulfonic acid (HEPES), 10 mM NaCl buffer solution (pH 7) to provide *p*pR and *p*pR/*p*HtrII complex embedded in Egg-PC lipid bilayers.

Solid-state NMR experiments

The fully hydrated sample was concentrated by centrifugation and packed into a 5.0 mm outer diameter (o.d.) zirconia pencil-type rotor with a tightly sealed glass cap. Solid-state NMR experiments were performed on a CMX-400 Infinity (Chemagnetics, Fort Collins, CO, USA) solid state NMR spectrometer equipped with an *in-situ* photo-irradiation NMR system using resonance frequencies of 400 and 100 MHz for ^{1}H and ^{13}C nuclei, respectively. ^{13}C cross-polarization magic-angle spinning (CP-MAS) experiments were performed using the following conditions: ^{13}C 90^{o} pulse of 5.4 μs, ^{1}H decoupling amplitude of 50 kHz, temperatures of -40 and -60°C and a MAS frequency of 4.0 kHz. TPPM proton high power decoupling was employed during each acquisition. ^{13}C chemical shifts were referenced to the carbonyl resonance of glycine powder at 176.03 ppm (tetramethylsilane (TMS) at 0.0 ppm).

***In-situ* photo-irradiation solid-state NMR measurements**

In-situ continuous photo-irradiation was carried out using an optical fiber passed from outside the magnet through a tightly scaled glass cap made from a glass rod glued to a zirconia rotor (28, 29, 32). The glass rod was grained so as to provide illumination perpendicular to the rotor wall. The fluid membrane proteins were attached

to the side wall of the rotor as a thin film and then light was directed perpendicular to the rotor wall from inside the spinner. If the irradiation is not perpendicular to the rotor wall, the light is completely reflected off the surface of the film sample and dose not penetrate into the sample. Use of CMX-400 Infinity NMR spectrometer equipped with this photo-irradiation system allowed us to efficiently irradiate samples in the rotor with green (520 nm) and blue (365 nm) LED light sources.

Stationary trapping of photo-intermediates using *in-situ* photo-irradiation solid-state NMR

In-situ photo-irradiation is particularly useful for studying the photo-cycle of several retinal binding membrane proteins. The half-life of the M-intermediate in *p*pR is approximately 1.7 s, which is much longer than that of the other intermediates, as shown in Figure 1(A). Thus, continuous irradiation of a sample with green light (520 nm) traps the M-intermediates in a stationary fashion, making it possible to detect relatively short-lived intermediates in the stationary state when their half-life differs from those of other intermediates (Figure 1(B)). The trapping efficiency can be increased by decreasing the temperature because the photoreaction is a thermal process except in photoillumination process (G → K), thereby extending the half-life of the

M-intermediates. The M-intermediates can be eliminated by illuminating with 365 nm LED light since the M-intermediates have a maximum absorbance frequency of 390 nm, which is different the absorbance frequencies from those of the other intermediates. The M-intermediates can therefore be selectively eliminated by directly irradiating with 365 nm blue light, allowing detection the activation of consecutive photoreaction processes, such as the double-photon process, by illuminating with multiple wavelengths. It is thus possible to select a particular intermediate by adjusting either temperature or wavelength.

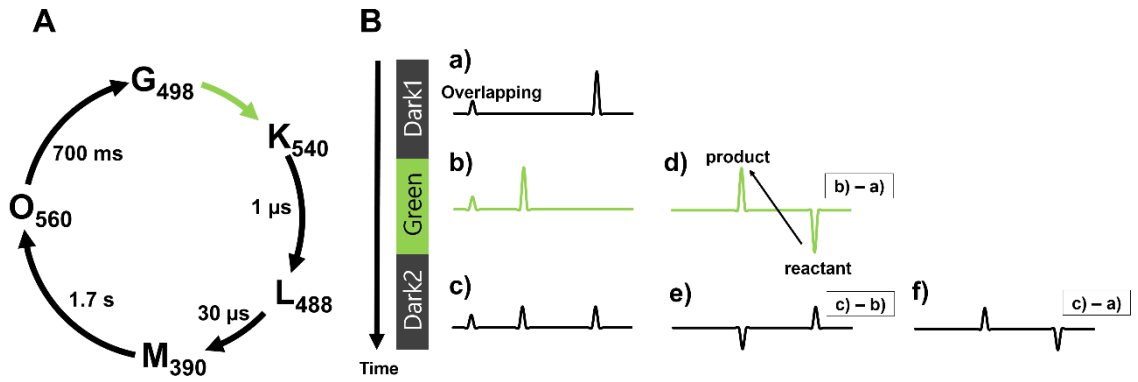

Figure 1. A. Typical photo-cycle of the *p*pR/*p*HtrII complex. The M- and O-intermediates have much longer half-lives than the K- and L-intermediates. B. Experimental protocol and strategy of analysis. Firstly, in-situ photo-irradiation solid-state NMR spectra were observed in the dark state (Dark1) (B(a)), then under illumination with green light (Green) (B(b)), and finally in the second dark

state (dark2) (B(c)). We analyzed the photoreaction pathway, and eliminated overlapping signals obtaining the difference spectra, the difference spectra was taken (B(d) = (b) – (a); B(e) = (c) – (b); B(f) = (c) – (a)). A negative peak in the difference spectrum indicates the reactant and a positive peak indicates a product.

Computational method

The ^{13}C chemical shift calculations were performed using the GIAO method (38–42) in the Gaussian09 (43) program with the B3LYP/6-311+g(2d,p) theory/basis set combination. The calculated chemical shifts were converted in ppm relative to TMS. A schematic structure of retinal, used in the chemical shift calculation, was shown in Scheme 1. Retinal binds to the protein through the side chain of Lys 205, included in the structure as shown in scheme 1. The Schiff base was considered to be as protonated in the calculation. The initial structure of the retinal was in the all-*trans* configuration of the crystal structure (pdb ID:1jgj) (44), which corresponds to the G state configuration. We investigated the configurations of the O- and N'-intermediates by evaluating the dependence of the ^{13}C NMR chemical shift on the configuration of retinal according to the rotation of the dihedral angles of 12C-13C=14C-15C, 14C-15C=Nζ-Cε, and 15C=Nζ-Cε-Cδ, abbreviated Φ, Ψ, and X, respectively (Scheme 1). The geometries of

the heavy atoms of retinal were fixed in each dihedral angle and only the hydrogen atoms were optimized with the same theory/basis set conditions before calculation of the chemical shift values.

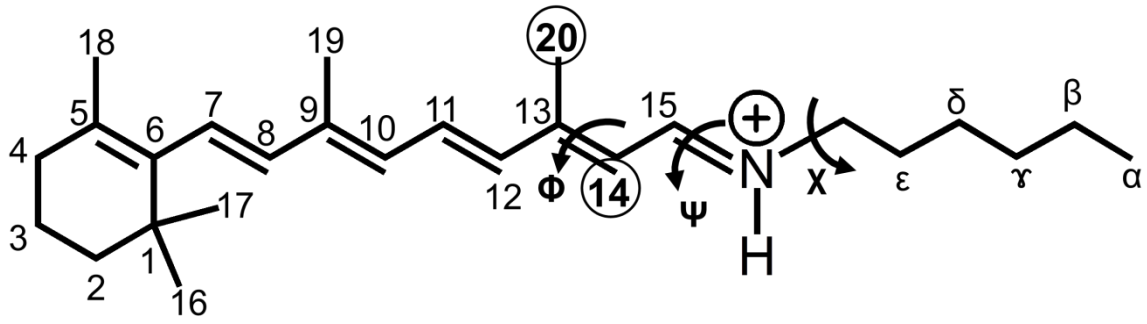

Scheme 1. Schematic structure of retinal covalently bonded through a Schiff base. The letters of α, β, γ, δ, ε are the positions of carbons of Lys205 in *p*pR. Circle numbers are the positions of carbons observed by ^{13}C CP-MAS solid-state NMR. The dihedral angles Φ, Ψ and χ were defined as 12C-13C=14C-15C, 14C-15C=Nζ-Cε, and 15C=Nζ-Cε-Cδ, respectively.

RESULTS AND DISCUSSION

Photoreaction pathways under the green light irradiation in *p*pR/*p*HtrII complex

In-situ photo-irradiation solid-state ^{13}C CP-MAS measurements were performed on the [20-^{13}C]-labeled-retinal-*p*pR/*p*HtrII complex at -40ºC. We obtained the photoreaction pathways under illumination with green light, by first observing the ^{13}C

CP-MAS NMR spectrum of the *p*pR/*p*HtrII complex in the dark condition (Dark1) at -40ºC (Figure 2A(a)) and then the ^{13}C CP-MAS spectrum under illumination with 520 nm green light (Figure 2A(b) to observe the intermediates in stationary state.

The [20-^{13}C] retinal signals shown in Figure 2A(a) and A(b) were heavily overlapped with the lipid signals. The difference spectrum (Green – Dark1) was therefore obtained as shown in Figure 2A(d), to analyze the photoreaction pathways induced by photo-irradiation. The difference spectrum between the dark and light irradiated states indicated that the negative peaks correspond to the reactant state and the positive peaks correspond to the product state. Thus, the ^{13}C CP-MAS NMR signal of the G-state at 13.5 ppm decreased and those of the M-intermediates at 22.1 ppm and 22.9 ppm (M1 and M2), the N'-intermediate at 23.9 ppm and the O-intermediate at 16.1 ppm, all increased. We discuss the assignment of the N'- and O-intermediates in the later section. As a result, the ^{13}C CP-MAS NMR signals of the [20-^{13}C] retinal-*p*pR/*p*HtrII complex show the process of transforming from the G-state (13.5 ppm) to a number of photo-intermediates. We previously reported that the G-state was transformed to three kinds of M-intermediates (M1, M2, M3) upon illumination with green light at -20ºC (28). In the present experiment at -40°C, we observed photo-intermediates in the 13-*cis* form (22.9, 22.1 ppm) assigned to M1 and M2 as we

reported previously (28), and to the N'-intermediate (23.8 ppm), newly assigned in this study, and the13-*trans* form (16.1 ppm) assigned to O-intermediate. In summary, the 13-*trans* form product peak at 16.1 ppm can be assigned to the O-intermediate and the 13-*cis* form can be assigned to the M-intermediates (22.1, 22.9 ppm) and the N'-intermediate (23.9 ppm), as discussed below. The chemical shift values are summarized in Table 1.

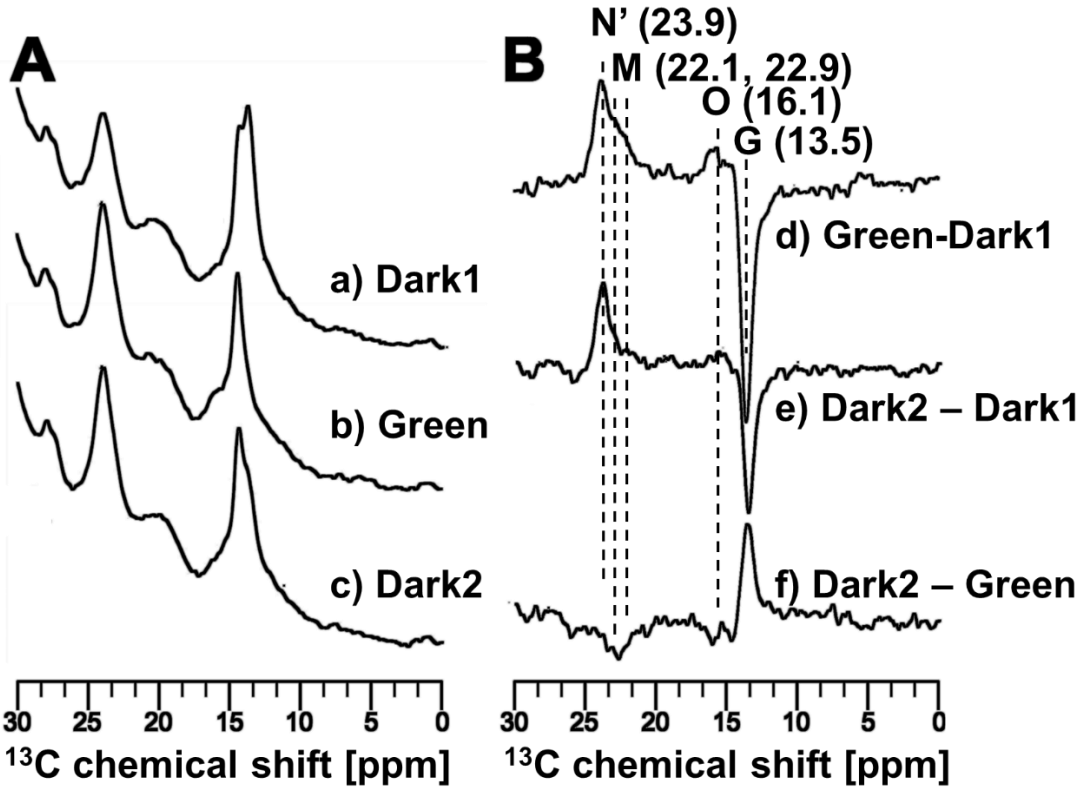

Figure 2. A. ^{13}C CP-MAS NMR spectra of the [20-^{13}C] retinal–*p*pR/*p*HtrII complex at -40ºC using 4 kHz MAS frequency, (a) acquired under initial dark conditions (Dark1), (b) acquired under irradiation with green light state (520 nm) (Green)

and (c) obtained one day after turning off irradiation (dark2). B. The difference spectra obtained by subtracting the ^{13}C CP-MAS NMR spectra, (d) obtained by Green – Dark1, (e) obtained by Dark2 – Dark1 and (f) obtained by Dark2 – Green.

Table 1 ^{13}C chemical shift values of retinal obtained from NMR experiment

		chemical shift [ppm]		Configuration
		20-^{13}C	14-^{13}C	
*p*pR/pHtrII(-40°C)	G-state	13.5		13-*trans*, 15-*anti*
	O-intermediate	16.1		13-*trans*
	M-intermediate	22.1, 22.9		13-*cis*, 15-*anti*
	N'-intermediate	23.9		13-*cis*
*p*pR (-40°C)	G-state	13.5	121.7	13-*trans*, 15-*anti*
	M-intermediate	22.3	126.8	13-*cis*, 15-*anti*
*p*pR(-60°C)	G-state	13.6	121.6	13-*trans*, 15-*anti*
	O-intermediate	16.4	115.4	13-*trans*
	M-intermediate	22.6	127.1	13-*cis*, 15-*anti*
	N'-intermediate	23.9	115.4	13-*cis*

Relaxation process from the green light irradiation state (Green) to the short dark state (Dark2)

The green light irradiation state was relaxed to the dark state by the process of thermal relaxation. Figure 2A(c) shows the ^{13}C CP-MAS NMR spectrum of *p*pR/*p*HtrII

complex obtained one day after terminating green light irradiation. The difference spectrum shown in Figure 2B(e) was obtained by subtracting the initial dark state (Dark1) from the second short dark state (Dark2). The peak at 23.9 ppm remained while the peaks at 22.1 and 22.9 ppm decreased. The difference spectrum shown in Figure 2B(f) was obtained by subtracting the green light illumination state (green) from the second short dark state (Dark2). The peaks at 22.1, 22.9 and 16.1 ppm decreased and G-state increased. These results indicate that the peak at 23.9 ppm is not due to the M-intermediates but rather to the N'-intermediate, and therefore the half-lives of the M-intermediates at 22.1 and 22.9 ppm and of the O-intermediate at 16.1 ppm are much shorter than that of the N'-intermediate at 23.9 ppm. Therefore, we conclude that the M- and O-intermediates relaxed to the G-state, and the N'-intermediate relaxed more slowly than the M- and O-intermediates.

Photoreaction pathway from the M-intermediates to the O-intermediate

A N-like intermediate with an absorbance maximum at 500 nm was previously observed in *pharaonis* phobohodopsin in the 13-*cis* form in a transient absorption study using azide to accelerate the decay of the M-intermediates (45). To confirm the existence of this N-like-intermediate, the sample in the present study was irradiated with

near-UV light at 365 nm to eliminate the M-intermediates (46), which have a maximum absorbance of 390 nm, after the accumulation of photo-intermediates by irradiation with 520 nm light.

Irradiation of the *p*pR/*p*HtrII complex with 520 nm green light at -40ºC converted the G-state to the O-, M- and N'-intermediates (Figure 2 and Figure 3A(a)). We found that the signal at 23.9 ppm did not decayed upon irradiation with 365 nm light irradiation (Figure 3A(b)). As described above, M-intermediates have an absorbance maximum at 390 nm due to the deprotonated Schiff base. Therefore, M-intermediates immediately decay upon illumination with 365 nm light (46) and then the remaining signal corresponding to the 13-*cis* form is assigned to the N'-intermediate (23.9 ppm).

After the M-intermediates of the *p*pR/*p*HtrII complex were trapped at -40ºC in a stationary manner by illumination with green light (Figure 3(a)), irradiation with LED light at 520 nm was switched to 365 nm (Figure 3A(b)). During this process, the intensities of the M-intermediates decayed while the intensities of the O-intermediate and the G-state increased (Figure 3(c)), whereas the N'-intermediate did not decay over the same period (Figure 3(b)). Furthermore, it is noted that the M-intermediates was transformed to the O-intermediate following irradiation with 365 nm blue light (Figure 3A(c)). The M-intermediates are reportedly transformed back to the G-state by

irradiation with blue light (365 nm) (46), since the M-intermediates have a maximum absorption of 390 nm. However, it was found that the M-intermediates are transformed to the O-intermediate upon irradiation with 365 nm light (Figure 3A(c)). As described above, spectroscopic evidence for the formation of an N'-intermediate was recently obtained in a transient absorption study (45), which reported that decay of the M-intermediates does not directly produce the N'-intermediate but rather produces an O-intermediate that is in equilibrium with the N'-intermediate. Based on previously reported finding and the results of the *in-situ* photo-irradiation solid-state NMR experiments, we summarize the photoreaction cycle of *p*pR/*p*HtrII complex as follows (Figure 4). The M-intermediates are converted to the O-intermediate under irradiation with 365 nm blue light through a double-photon process, and the O-intermediate is then converted to the N'-intermediate until an equilibrium state is achieved in which the intensity of the N'-intermediate is higher than that of the O-intermediate (Figure 3A(b)).

Double-photon process from the G-state to the O-intermediate

We found the transform process from the G-state to the O-intermediate by observing the difference ^{13}C CP-MAS spectrum obtained by the blue light irradiation to the G-state. The ^{13}C CP-MAS NMR spectrum measurement of [20-^{13}C]

retinal-*p*pR/*p*HtrII complex was first performed under initial dark conditions (Dark1) at -40ºC. Upon switching directly from the initial dark condition (Dark1) to 365 nm blue light illumination, the M-intermediates were converted to the O-intermediate through a double-photon process (Figure 3B(d)). Consequently, the O-intermediate was converted to the N'-intermediate until an equilibrium state (Figure 3B(e)). This pathway was clearly observed in the difference spectrum generated by subtracting the blue light illumination state from the Dark2 state (Figure 3B(f)).

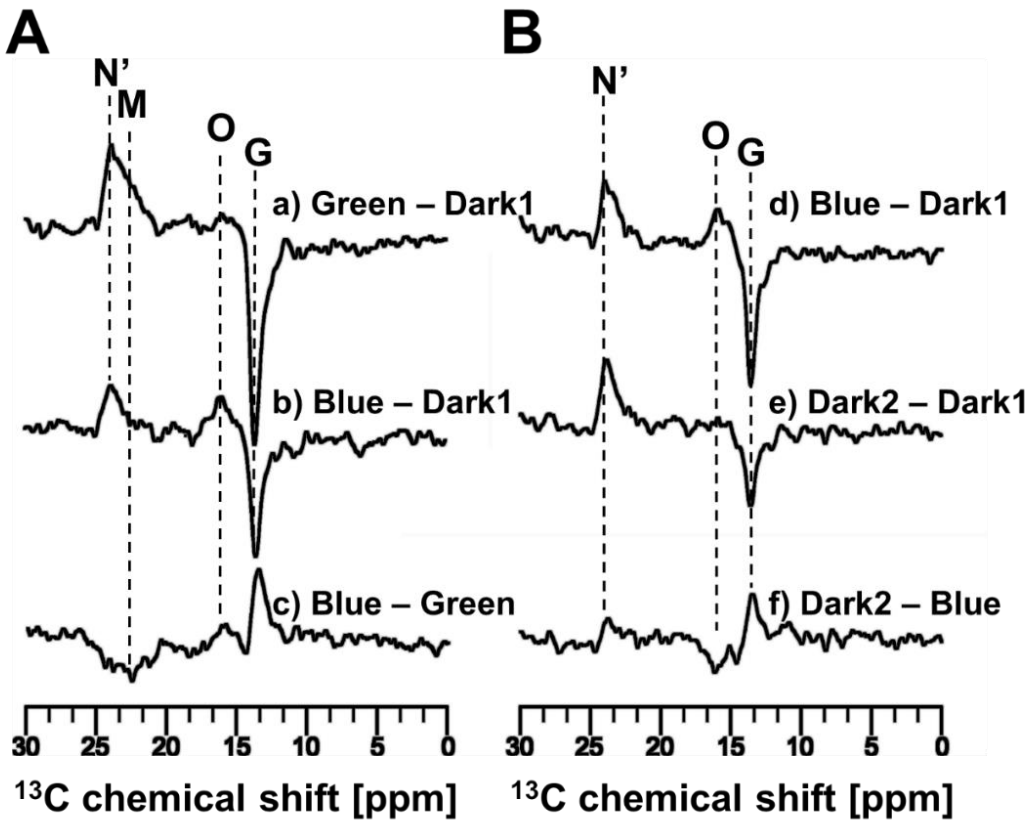

Figure 3. ^{13}C CP-MAS NMR difference spectra of the [20-^{13}C] retinal labeled

ppR/pHtrII complex were measured at -40 °C using 4 kHz MAS. A. (a) The difference spectrum obtained by subtracting the initial dark conditions (Dark1) from the green light illumination state (Green) (Green – Dark1). (b) The difference spectrum obtained by subtracting the initial dark conditions (Dark1) from the blue light illumination state (Blue) after the green light stationary state Blue – Dark1. (c) The difference spectra obtained by Blue – Green, which is identical with (b) – (a). B. (d) The difference spectrum obtained by subtracting the initial dark conditions (Dark1) from the blue light illumination state (Blue) (Blue – Dark1). (e) The difference spectrum obtained by subtracting the initial dark conditions (Dark1) from the second dark conditions (Dark2) after turning off irradiation (Dark2 – Dark1). (f) The difference spectra obtained by subtracting Blue from Dark2 (Dark2 – Blue), which is identical with (e) – (d).

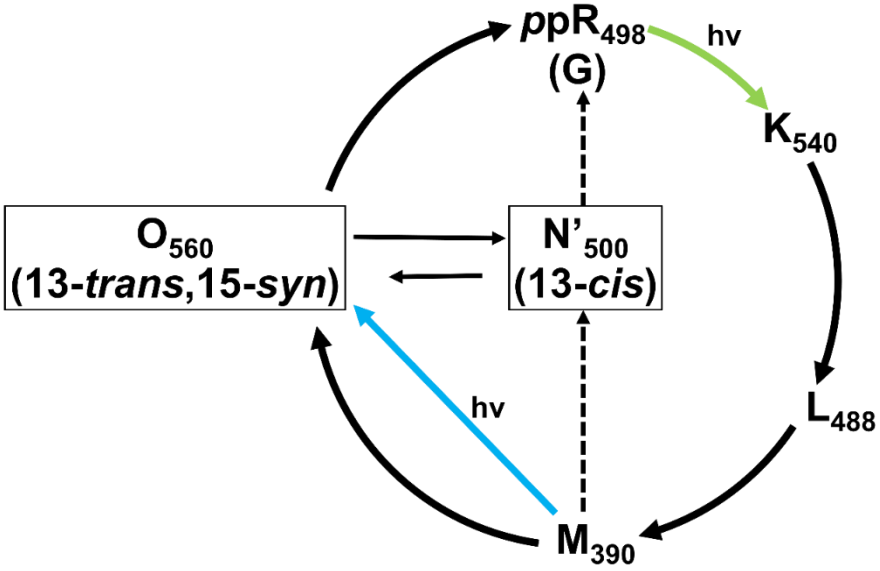

Figure 4. The photo reaction pathway of ppR including the N'-intermediate, as

revealed by *in-situ* photo-irradiation solid-state NMR measurements. The O-intermediate is in an equilibrium state to with the N'-intermediate. The λ maximum of the N'-intermediate was estimated at 500 nm (45). The transition process from the M-intermediates to the O-intermediate is shown by a blue arrow. The pathway for the thermal relaxation from the M-intermediates to the N'-intermediate, and subsequently from the N'-intermediate to the G-state, remain unclear and thus are designated with a black dashed arrow. The general configurations of the O- and N'-intermediates were the 13-*trans*, 15-*syn*, and the 13-*cis* forms, respectively.

Photo-reaction pathways of *p*pR from the G-state to the M-intermediates at -40°C

We obtained the ^{13}C CP-MAS NMR signals of [20-^{13}C] retinal-*p*pR without *p*HtrII reconstituted in Egg-PC under the initial dark conditions (Figure 5A(a)) followed by green light illumination with a 520 nm LED (Figure 5A(b)). The difference spectrum (Figure 5A(c)) between the M-intermediates and the G-state (Figure 5A(a) - A(b)) indicated the transformation process from the G-state to the M-intermediate.

The ^{13}C CP-MAS NMR spectra of [20-^{13}C] retinal-*p*pR in the green light illumination with a 520 nm LED (Figure 5B(a)) and in the subsequent dark condition (Dark2) (Figure 5B(b)), and the difference spectrum (Figure 5B(c)) between the dark2

condition and the green light condition (Figure 5B(a) - B(b)), indicated that the M-intermediate transformed to the G-state via a thermal relaxation decay process at -40°C in *p*pR alone.

The ^{13}C NMR spectra of [14-^{13}C] retinal-*p*pR (Figure 5C and D) and the difference spectrum also indicated the process G-state → M-intermediate → G-state, as for [20-^{13}C] retinal-*p*pR. In addition, the chemical shift values of [14-^{13}C] retinal-*p*pR were 121.7 ppm (G-state) and 126.8 ppm (M-intermediate) at -40°C (Table 1).

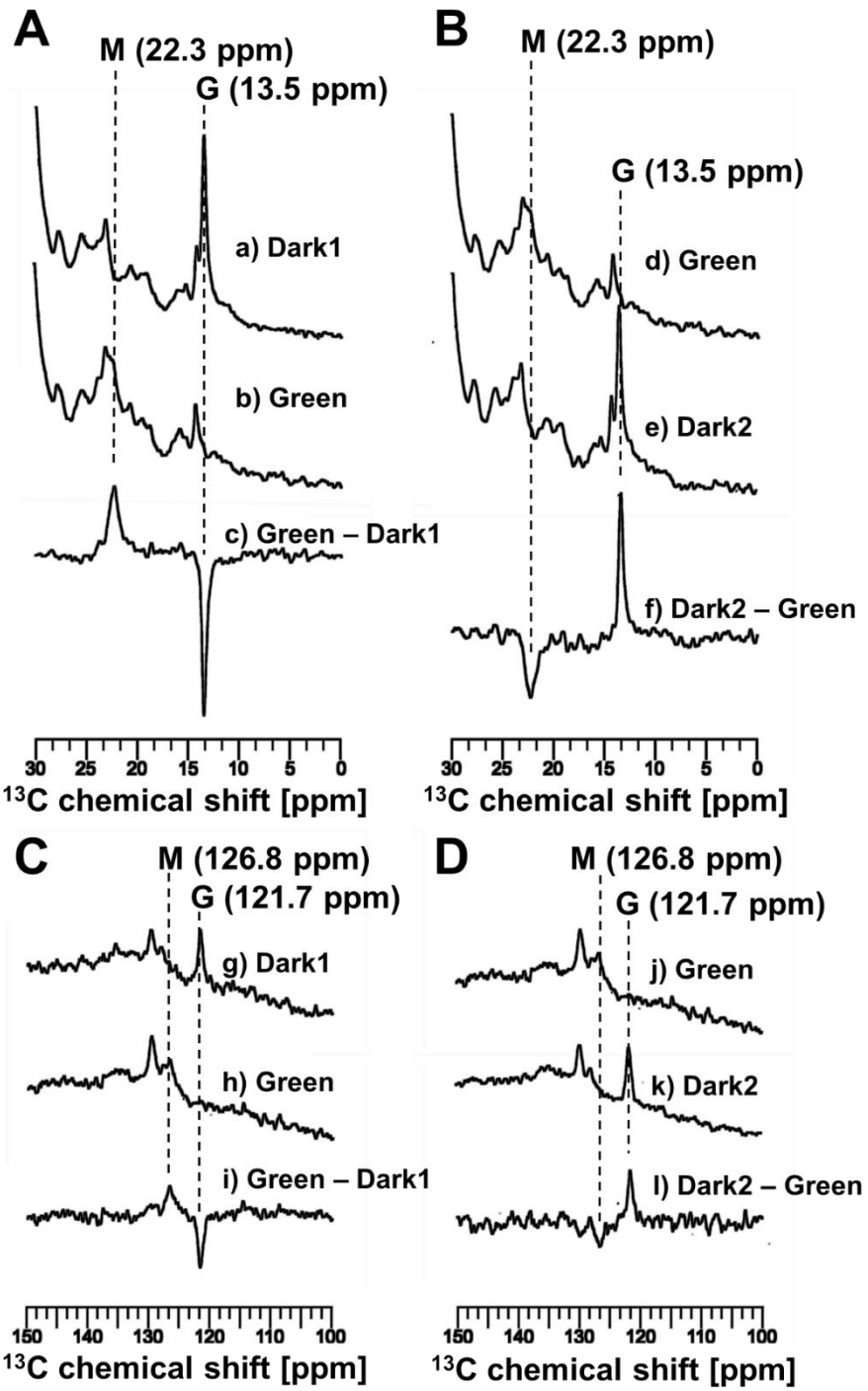

Figure 5. ^{13}**C CP-MAS NMR spectra of [20-**^{13}**C, 14-**^{13}**C] retinal-*p*pR without *p*HtrII at -40°C under 4 kHz MAS. A.** ^{13}**C NMR spectra of [20-**^{13}**C] retinal-*p*pR indicated the transformation process from the G-state (13.5 ppm) to the M-intermediate**

(22.3 ppm), (a) acquired under initial dark conditions (Dark1), (b) acquired under green light illumination states (Green), and (c) the difference spectrum obtained by subtracting the initial dark conditions (Dark1) from the green light illumination state (Green) (Green – Dark1). B. ^{13}C NMR spectra of [20-^{13}C] retinal-*p*pR showing the thermal relaxation process from the M-intermediate to the G-state, (d) acquired under green light illumination states (Green), (e) acquired under short dark conditions (Dark2) after turning off irradiation, and (f) the difference spectrum obtained by subtracting the green light illumination state (Green) from the second conditions (Dark2). (Dark2 – Green). C. ^{13}C NMR spectra shown the region from 100.0 ppm to 150.0 ppm for the same experiment as A, (g) acquired under initial dark conditions (Dark1), (h) acquired under green light illumination states (Green), and (i) the difference spectrum obtained by subtracting the initial dark conditions (Dark1) from the green light illumination state (Green) (Green – Dark1). D. ^{3}C NMR spectra shown the region from 100.0 ppm to 150.0 ppm for the same experiment as B, (j) acquired under green light illumination states (Green), (k) acquired under short dark conditions (Dark2) after turning off irradiation, and (l) the difference spectrum obtained by subtracting the green light illumination state (Green) from the second conditions (Dark2). (Dark2 – Green). The spectra shown C and D indicated the transformation process from G-state (121.7 ppm) to M-intermediate (126.8 ppm) and the thermal decay process.

Photoreaction pathways from the M-intermediate to the O-intermediate in *p*pR

As discussed in the above section regarding the *p*pR/*p*HtrII complex, the M-, N'- and O-intermediates were observed under continuous green light illumination at 520 nm at -40°C as for the *p*pR/*p*HtrII complex. And then, in the *p*pR alone without *p*HtrII, the N'- and O-intermediates could not be trapped at -40°C. We anticipated that the life-lives of late photo-intermediates such as the N'- and O-intermediates will be elongated at the lower temperature due to decreased mobility of the protein. As expected, these intermediates were successfully trapped at -60°C (Figure 6A(a)).

In-situ photo-irradiation solid-state ^{13}C CP-MAS measurements were performed on [20-^{13}C] retinal-*p*pR alone at -60°C, and the results were identical as for the *p*pR/*p*HtrII complex at -40°C. Under illumination with green light, the difference ^{13}C CP-MAS NMR spectrum of [20-^{13}C] retinal-*p*pR (green light illumination (Green) – initial dark condition (Dark1)) indicated the transformation process from the G-sate (13.6 ppm) to the O-, M- and N'-intermediates (16.4, 22.3 and 23.9 ppm) (Figure 6A (a)). After stationary trapping of these photo-intermediates, the light source was switched from 520 nm to blue light at 360 nm. The result indicated that the signal of the M-intermediates (22.6 ppm) decreased and the signal of the O-intermediate (16.4 ppm) increased (Figure 6A(b)). The absorbance maximum of the M-intermediate was 395 nm

and thus this result indicated that the M-intermediates were transformed to the O-intermediate at an accelerated rate by irradiation with 365 nm blue light. This photo-reaction pathway was clearly observed in the difference spectrum, subtracting the green light illumination state from the blue light illumination sate (Figure 6A(c)).

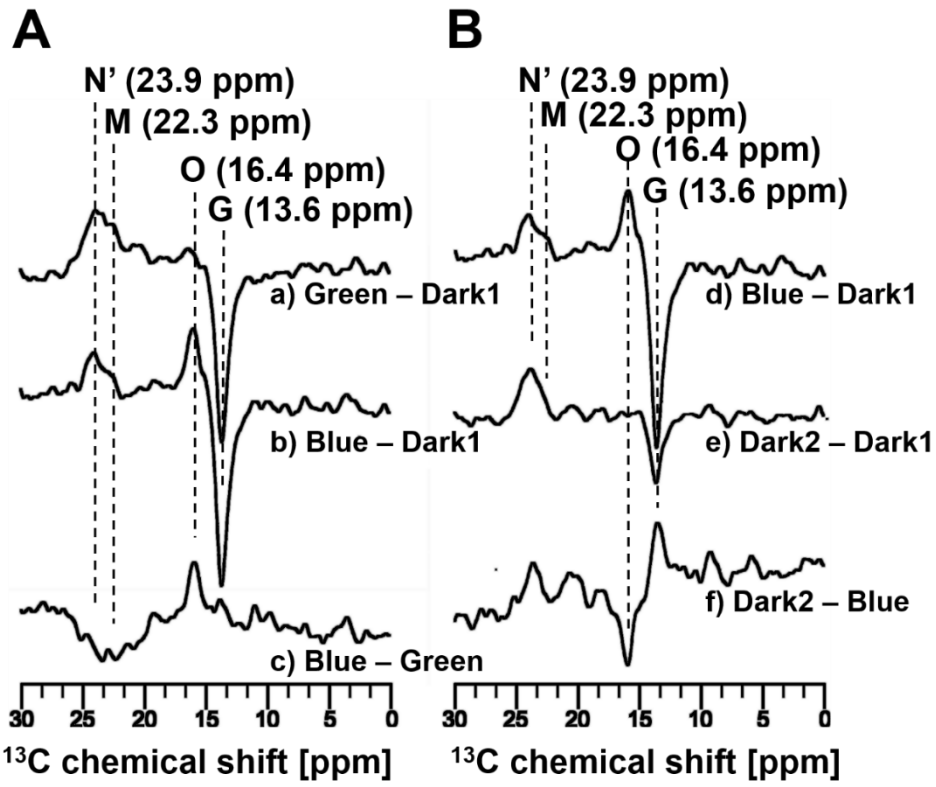

Figure 6. ^{13}C CP-MAS NMR signals of [20-^{13}C]retinal-*p*pR alone at -60°C under 4 kHz MAS. A. The difference spectra of the [20-^{13}C] retinal-*p*pR obtained, (a) by subtracting the initial dark conditions (Dark1) from the green light illumination states (Green) (Green – Dark1), (b) Blue – Dark1 and (c) Blue – Green. The difference spectrum shown (a) indicates that the transformation process from the G-state (13.6 ppm) to M (22.3 ppm), N' (23.9 ppm) and O-intermediates (16.4 ppm)

upon the green light illumination. The difference spectra shown (b) and (c) indicate that we successfully trapped O-intermediate (16.4 ppm) upon the subsequently blue light illumination. B. The difference spectra of the [20-^{13}C] retinal-*p*pR obtained, (d) by subtracting the initial dark conditions (Dark1) from the blue light illumination state (Blue) (Blue – Dark1), (e) by subtracting the short dark conditions after turning off irradiation (Dark2) (Dark2 – Dark1) and (f) Dark2 – Blue.

Relaxation process from the O-intermediate to the N'-intermediate.

We obtained the relaxation process from the O-intermediate to the N'-intermediate, by observing the different spectra shown Figure 6B. The difference ^{13}C CP-MAS NMR spectrum of [20-^{13}C] retinal-*p*pR between the blue state (Blue) and initial dark conditions (Dark1) indicated the product photo-intermediates were the O- and N'-intermediates in the blue light illumination state. By turning off the irradiation, the O-intermediate was converted to the N'-intermediate, as with *p*pR/*p*HtrII complex (Figure 6B(e)). This pathway was clearly observed in the difference spectrum generated by subtracting the blue light illumination state from the Dark2 state (Figure 6B(f)).

Chemical shift values of [14-^{13}C] retinal for the intermediates in *p*pR

We revealed the configurations of the O- and N'-intermediate by measuring the C CP-MAS NMR spectra of [14-^{13}C] retinal-*p*pR. The chemical shift values of [14-^{13}C] retinal contain important information regarding the 15-s*yn*/*anti* configuration (19, 32). The spectra shown in Figure 7 show the region from 100.0 ppm to 150.0 ppm for the same experiments as shown in Figure 6 and indicates the chemical shifts of [14-^{13}C] retinal-*p*pR. At -60°C, *in-situ* photo-irradiation solid-state ^{13}C CP-MAS spectra were observed for [14-^{13}C] retinal-*p*pR and the signal at 127.1 ppm was assigned to [14-^{13}C] retinal in the M-intermediate states resulting from a transformation process from the G-sate to the M-intermediates under green light illumination with 520 nm LED light (Figure 7A(a)). Subsequent blue light illumination with 365 nm light resulted in an intense signal from the O-intermediate, as with the signal of the [20-^{13}C] retinal-*p*pR shown Figure 6. Therefore, the main positive peak in the difference spectrum (Figure 7 A(b)) was assigned to the O-intermediate and the chemical shift value of [14-^{13}C] retinal was 115.4 ppm. As discussed above, the M-intermediates transforms to the O-intermediate by the blue light illumination and thus the chemical shift value at 115.4 ppm was indeed due to the O-intermediate (Figure 7A(c)). The spectrum shown in Figure 7B(d) also indicated that the 115.4 ppm signal is assignable to the O-intermediate due to the double photon process from the G-state to the O-intermediate

upon blue light illumination.

The difference spectrum shown in Figure 7B(e) clearly indicated that the 115.4 ppm signal also belonged to the N'-intermediate because the N'-intermediate showed a very long life and the signal intensity remained unchanged at -60 °C as shown in Figure 6(b, e). In addition, the thermal relaxation pathway of the O-intermediate was observed as a decrease in the signal at 115.4 ppm (Figure 7B(f)).

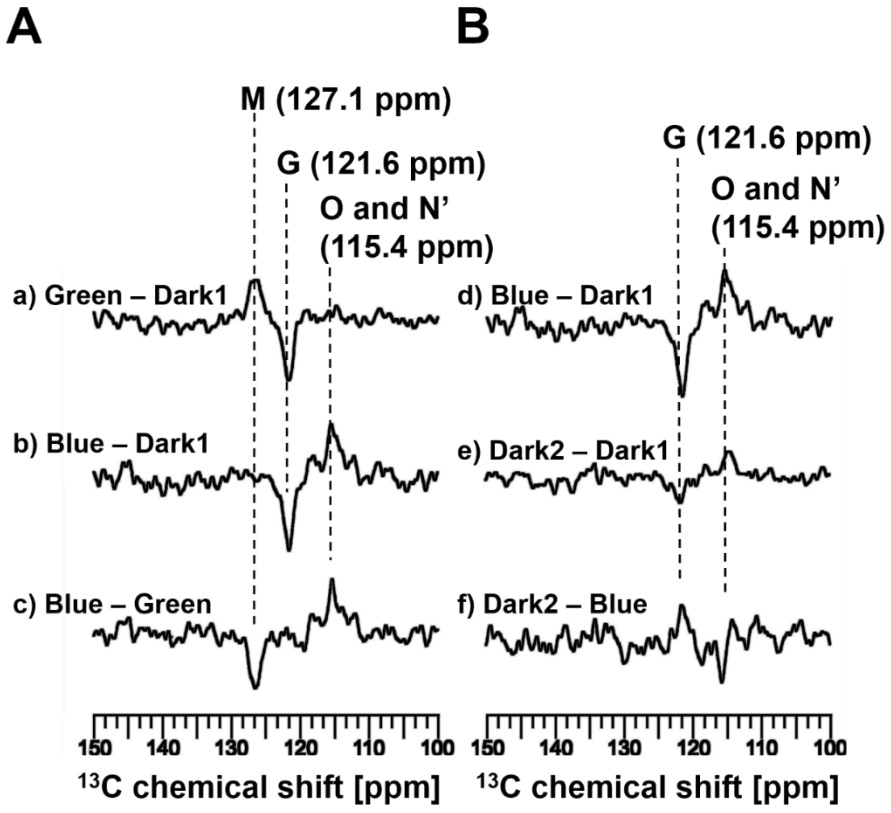

Figure 7. ^{13}C CP-MAS NMR signals of [14-^{13}C] retinal-*p*pR alone at -60°C under 4 kHz MAS. A. The difference spectra of the [14-^{13}C] retinal-*p*pR obtained (a) by subtracting the initial dark conditions (Dark1) from the green light illumination

states (Green) (Green – Dark1), (b) Blue – Dark1 and (c) Blue – Green. The difference spectrum shown (a) indicates that the transformation process from the G-state (121.6 ppm) to the M-intermediates (127.1 ppm) upon the green light illumination. The difference spectra shown (b) and (c) indicate that the transition process from the M-intermediates to the O-intermediate (115.4 ppm) upon the subsequently blue light illumination. B. The difference spectra of the [14-^{13}C] retinal-*pp*R obtained, (d) by subtracting the initial dark conditions (Dark1) from the blue light illumination state (Blue) (Blue – Dark1), (e) by subtracting the short dark conditions after turning off irradiation (Dark2) (Dark2 – Dark1) and (f) Dark2 – Blue. The difference spectra shown in (e) and (f) indicate that the remaining signal at 115.4 ppm also belongs the N'-intermediate.

Conformation of retinal in the late photo-intermediates

We have assigned the ^{13}C NMR chemical shift values for the late photo-intermediates M-, O- and N'-intermediates (Table 1). The configuration of the M-intermediates was clearly shown to be 13-*cis*,15-*anti* by comparing the present result with previous studies of Salinibacter sensory rhodopsin I (SrSRI), bR and its mutant Y185F-bR (19, 29, 32). (Table S1). Furthermore, the deprotonated Schiff base state in the M-intermediates was obtained as a result of the fast transformation process initiated by blue light illumination. This comparison and our previous studies in *pp*R and SrSRI

(28, 29) allow the 13C=14C configuration of retinal in the O- and N'-intermediates to be assigned to the 13-*trans* and 13-*cis* forms, respectively. The 15C=Nζ configuration is more challenging because the value of 115.4 ppm is the boundary region between the 15-*syn* and 15-*anti* forms. For example, in the study of Y185F-bR, the CS* intermediate has been assigned to the15-*syn* form and the chemical shift value of [14-^{13}C] retinal was 115.3 ppm (32). On the other hand, the N-intermediate of wt-bR has been assigned to the15-*anti* form and the chemical shift value of [14-^{13}C] retinal was 115.2 ppm (47) (Table S1). The following is a detailed discussion of the configurations of the O- and N'-intermediates as elucidated by DFT calculation.

Determination of the dihedral angles Φ for the O- and N'-intermediates

We elucidated the configuration of the O- and N'-intermediates by investigating the relationship between the ^{13}C NMR chemical shift values and configuration by using the DFT calculation. The crystal structure (pdb ID:1jgj) (44) corresponding to the G state was used as a starting configuration, and has the dihedral angles Φ = -177°, Ψ = -175° and X = -66°. The chemical shift values of 20-^{13}C and 14-^{13}C for this configuration were calculated to be 17.5 and 128.1 ppm, respectively, and these values are shown in Table 2. Touw et al. (48) previously calculated the chemical shift at 20-^{13}C

for all-*trans*-retinal to be 18.0 ppm (48), which is very similar to the value obtained in this work. However, these calculated values show some discrepancy with the experimental values, of 13.6 and 121.6 ppm, with the calculated chemical shift values being 3.9 and 6.5 ppm larger values than the experimental 20-^{13}C and 14-^{13}C values, respectively. Touw et al. (48) also showed the similar discrepancy. Therefore, in the following discussion, the calculated values will be discussed with corrected values by adding 3.9 and 6.5 ppm to the experimental values for 20-^{13}C and 14-^{13}C in retinal, respectively.

The dependence of the chemical shift value of 20-^{13}C in retinal on the dihedral angles Φ and Ψ were investigated and the results were shown in Figure 8(A) and (B), respectively. The chemical shift at 20-^{13}C in retinal drastically changes according to the rotation of dihedral angle Φ but it is almost independent of the change in the dihedral angle Ψ. These results indicate that the value of 20-^{13}C can be used to determine the configuration with dihedral angle Φ. The experimental chemical shift values of 20-^{13}C for the O- and N'-intermediates were 16.4 and 23.9 ppm and thus the corrected values of these conformations should be 20.3 and 27.8 ppm, respectively. The positions of these values were shown in Figure 8(A). The corresponding dihedral angle Φ for the O-intermediate configuration was estimated as -150° and for the N'-intermediate it was

estimated as -63°, as shown in Table 2.

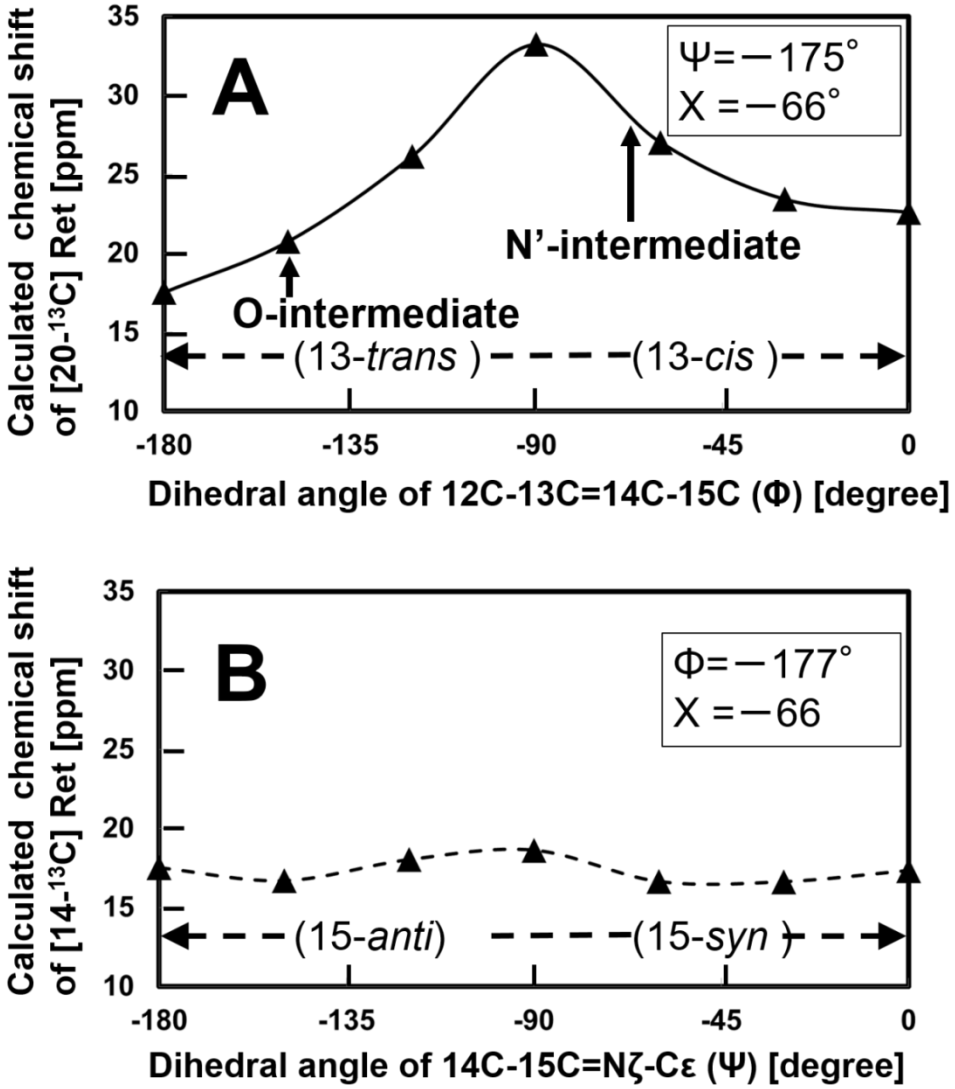

Figure 8. The dependency of the chemical shift value of 20-^{13}C in retinal on the dihedral angles Φ and Ψ is shown in (A) and (B), respectively. In (A), only the dihedral angle Φ was rotated from the *trans* (-180º) to the *cis* (0º) configuration by setting Ψ and X at -175° and -66º, respectively (44)**. In (B), only the dihedral angle Ψ was rotated from the *anti* (-180º) to the *syn* (0º) configuration by fixing Φ and X**

to -177° and -66°, respectively (44)**. The calculated chemical shift values were converted to ppm from TMS.**

Table 2 ^{13}C chemical shift values of retinal calculated by DFT, and the conformation of retinal in several photo-intermediates.

	Chemical shift [ppm]		Dihedral angle [degree]			Configuration
	20-^{13}C	14-^{13}C	Φ	Ψ	χ	
G-state	17.5	128.1	-177[a]	-175 [a]	-66 [a]	13-*trans*, 15-*anti*
O-intermediate	20.3	121.9	-150	0	-180	13-*trans*, 15-*syn*
N'-intermediate	27.8	121.9	-63	-175	-180	13-*cis*, 15-*anti*
				-7	-180	13-*cis*, 15-*syn*
				-175	-66[a]	13-*cis*, 15-*anti*

Ref. (44) (pdb ID:1JGJ)

Determination of the dihedral angle Ψ for the O-intermediate

The dihedral angle Φ in the O-intermediate was estimated to be -150° and thus the dihedral angle Ψ was investigated on this intermediate next and the dependence of the chemical shift value of 14-^{13}C in retinal on the dihedral angle Ψ was evaluated by

setting Φ at -150° and X at -66°. The results were shown in Figure 9 (dashed line) and showed that the chemical shift value for the 15-*syn* form was larger than that of the 15-*anti* form. However, previous experiments showed opposite. For example, the values of 14-^{13}C for 15-*anti* and 15-*syn* were 122.0 ppm and 110.5 ppm for bR as shown in Table S1 and thus the calculated chemical shift of the *syn*-state should be up-field compared to that of the *anti*-state.

We resolved this discrepancy by conducting calculations using the *trans* configuration for dihedral angle **X** (**X** = -180°) because in this configuration we would expected a γ-effect between the 14-^{13}C proton and the ε proton(49)(49). The results were also shown in Figure 9 and indicate that the chemical shift value of 14-^{13}C in the *syn* conformation (Ψ = 0°) changed by -4.0 ppm from anti (Ψ = -180°) configuration (Figure 9, (dashed line)). This change in chemical shift allowed estimation of the configuration of the O-intermediate. The experimental chemical shift values of 14-^{13}C of the O-intermediate was 115.4 ppm, as summarized in Table 1, and thus the offset value of this configurations should be 121.9 ppm, corresponding to a dihedral angle Ψ of 0°. The configuration of the O-intermediate can thus be determined to have the dihedral angles Φ and Ψ of -150° and 0°, respectively, as listed in Table 2. These results indicated that the configuration of the O-intermediate was, in general, in the 13-*trans*

and 15-*syn* form.

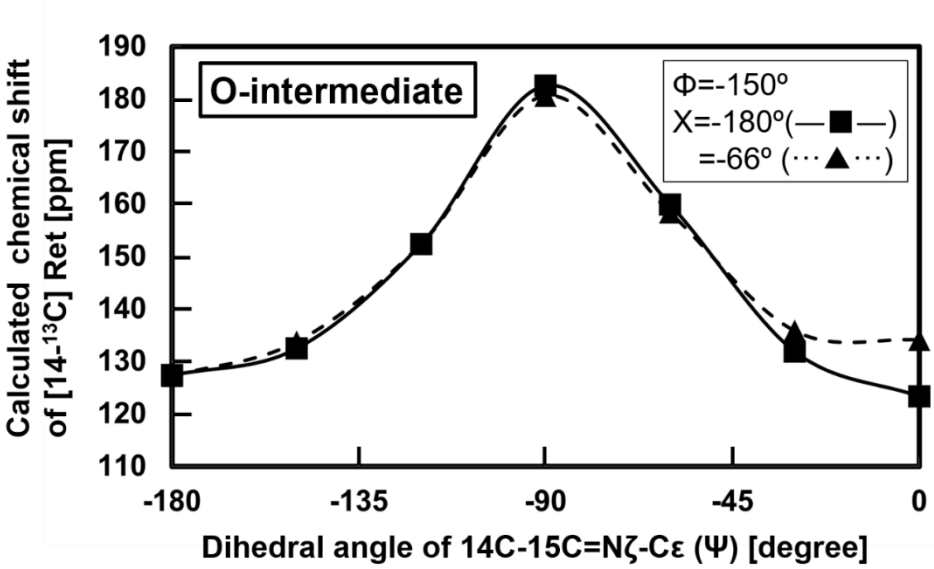

Figure 9. The chemical shift value of 14-^{13}C in retinal was calculated by changing the dihedral angle Ψ. The Φ angle was fixed at -150°, as estimated for the O-intermediate conformation discussed in Figure 6. The X angle was set at the crystal conformation (44) of -66° in (▲), and at trans conformation (44) of -180° in (■).

Determination of the dihedral angle Ψ for the N'-intermediate

The dihedral angle of Ψ was estimated in a manner similar to that discussed above. The conformation of the N'-intermediate was calculated using the dependence of the chemical shift value of 14-^{13}C in retinal on the dihedral angles Ψ and the results

were shown in Figure 10. The dihedral angle Φ in the N'-intermediate was set at -63° as estimated in Figure 8(A). Two sets of values were used in the calculations for the dihedral angle X: the crystal value of -66° and the *trans* form value of -180°, and both the results were shown in Figure 10. The curves of the chemical shifts allowed estimation of the conformation of the N'-intermediate. The chemical shift value of ^{13}C of the N'- intermediate was 115.4 ppm as summarized in Table 1 and thus the offset value of this conformation should be 121.9 ppm. However, three points correspond to the dihedral angle Ψ in Figure 10: the dihedral angles Ψ and X are (Ψ = -175° and X = -66°), (Ψ = -175° and X = -180°), and (Ψ = -17° and X = -180°). Although the dihedral angle Φ in the N'-intermediate was determined as -63°, the remaining dihedral angles Ψ and X could be any of these three possibilities.

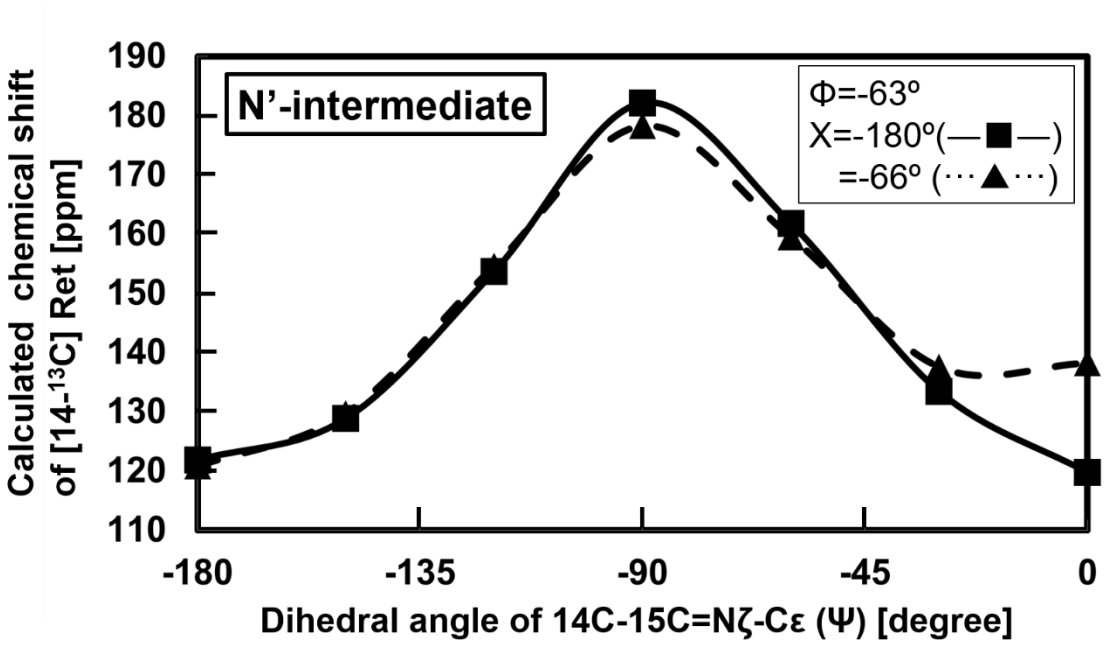

Figure 10. The chemical shift value of 14-^{13}C in retinal was calculated by changing the dihedral angle Ψ and fixing Φ at -63°, as estimated for the N'-intermediate configuration discussed in Figure 6. The X angle was set at the crystal configuration (44) of -66° in (▲) and the *trans* conformation (44) of -180° in (■).

CONCLUSION

We observed the M-, O- and N'-intermediates from *p*pR and *p*pR/*p*HtrII complex reconstituted in Egg-PC membrane by irradiation with green light using *in-situ* photo-irradiation solid-state NMR. Changes in the ^{13}C CP-MAS NMR signals resulting from switching the wavelength of light used for continuous irradiation from 520 nm to

365 nm, revealed the pathways of the late photo-active intermediates from the M-intermediates to the O-intermediate. Interestingly, one of the multiple M-intermediates previously reported was identified as an N-like-intermediate reported in bR which we designated the N'-intermediate. We suggest that the N'-intermediate might play important roles in signaling as a pre-amplitude mechanism because it has a long life similar to the O-intermediate. Detailed configurations of the O- and N'-intermediates were revealed by NMR experiments and DFT calculation and showed that the chemical shift values of [14-^{13}C] retinal are useful for determining the 15-*syn*, *anti* configuration.

ACKNOWLEDGMENTS

This work was supported by Grants-in-Aid for Scientific Research in an Innovative Area (16H00756 to AN, 25104005 to YS and 16H00828 to IK), and by a grant-in-aid for Scientific Research (C) (15K06963 to AN) and Research (B) (15H04363 to YS and 15H04336 to IK) and a Grant-in-Aid for JSPS Research Fellow (16J00073 to YM) from the Ministry of Culture, Sports, Science and Technology of Japan. This work was also supported by JST-CREST and AMED to YS. The authors thank the Research Center for Computational Science, Okazaki, Japan, for use of their

computing facilities to perform a part of the calculation described in this paper.

REFERENCES

1. Govorunova, E.G., O.A. Sineshchekov, H. Li, and J.L. Spudich. 2017. Microbial Rhodopsins: Diversity, Mechanisms, and Optogenetic Applications. Annu Rev Biochem. 86: 845–872.
2. Hoff, W.D., K.-H. Jung, and J.L. Spudich. 1997. Molecular mechanism of photosignaling by archaeal sensory rhodopsins. Annu. Rev. Biophys. Biomol. Struct. 26: 223–258.
3. Spudich, J.L., and Hh. Luecke. 2002. Sensory rhodopsin II: functional insights from structure. Curr. Opin. Struct. Biol. 12: 540–546.
4. Suzuki, D., H. Irieda, M. Homma, I. Kawagishi, and Y. Sudo. 2010. Phototactic and chemotactic signal transduction by transmembrane receptors and transducers in microorganisms. Sensors. 10: 4010–4039.
5. Inoue, K., T. Tsukamoto, and Y. Sudo. 2014. Molecular and evolutionary aspects of microbial sensory rhodopsins. Biochim. Biophys. Acta - Bioenerg. 1837: 562–577.
6. Kamo, N., K. Shimono, M. Iwamoto, and Y. Sudo. 2001. Photochemistry and Photoinduced Proton Transfer by Pharaonis Phoborhodopsin. Biochem. 66: 1277–1282.
7. Imamoto, Y., Y. Shichida, J. Hirayama, H. Tomioka, N. Kamo, and T. Yoshizawa. 1992. Chromophore Configuration of Pharaonis Phoborhodopsin and Its Isomerization on Photon Absorption. Biochemistry. 31: 2523–2528.
8. Gordeliy, V.I., J. Labahn, R. Moukhametzianov, R. Efremov, J. Granzin, R. Schlesinger, G. Büldt, T. Savopol, A.J. Scheidig, J.P. Klare, and M. Engelhard. 2002. Molecular basis of transmembrane signalling by sensory rhodopsin

II-transducer complex. Nature. 419: 484–487.

9. Shimono, K., T. Hayashi, Y. Ikeura, Y. Sudo, M. Iwamoto, and N. Kamo. 2003. Importance of the broad regional interaction for spectral Tuning in natronobacterium pharaonis phoborhodopsin (sensory rhodopsin II). J. Biol. Chem. 278: 23882–23889.

10. Sudo, Y., Y. Furutani, H. Kandori, and J.L. Spudich. 2006. Functional importance of the interhelical hydrogen bond between Thr ^{204} and Tyr^{174} of sensory rhodopsin II and its alteration during the signaling process. J. Biol. Chem. 281: 34239–34245.

11. Sudo, Y., Y. Furutani, A. Wada, M. Ito, N. Kamo, and H. Kandori. 2005. Steric constraint in the primary photoproduct of an archaeal rhodopsin from regiospecific perturbation of C-D stretching vibration of the retinyl chromophore. J. Am. Chem. Soc. 127: 16036–16037.

12. Wegener, A.A., I. Chizhov, M. Engelhard, and H.J. Steinhoff. 2000. Time-resolved detection of transient movement of helix F in spin-labelled pharaonis sensory rhodopsin II. J. Mol. Biol. 301: 881–891.

13. Spudich, J.L. 1998. Variations on a molecular switch: Transport and sensory signalling by archaeal rhodopsins. Mol. Microbiol. 28: 1051–1058.

14. Yoshida, H., Y. Sudo, K. Shimono, M. Iwamotoa, and N. Kamo. 2004. Transient movement of helix F revealed by photo-induced inactivation by reaction of a bulky SH-reagent to cysteine-introduced pharaonis phoborhodopsin (sensory rhodopsin II). Photochem. Photobiol. Sci. 3: 537–542.

15. Moukhametzianov, R., J.P. Klare, R. Efremov, C. Baeken, A. Göppner, J. Labahn, M. Engelhard, G. Büldt, and V.I. Gordeliy. 2006. Development of the

signal in sensory rhodopsin and its transfer to the cognate transducer. Nature. 440: 115–119.

16. Ernst, O.P., D.T. Lodowski, M. Elstner, P. Hegemann, S.B. Leonid, and H. Kandori. 2014. Microbial and Animal Rhodopsins : Structures, Functions and Molecular Mechanisms. Chem. Rev. : 1–7.

17. Smith, S.O., H.J.M. de Groot, R. Gebhard, J.M.L. Courtin, J. Lugtenburg, J. Herzfeld, and R.G. Griffin. 1989. Structure and Protein Environment of the Retinal Chromophore in Light- and Dark-Adapted Bacteriorhodopsin Studied by Solid-State NMR. Biochemistry. 28: 8897–8904.

18. McDermott, A.E., L.K. Thompson, C. Winkel, M.R. Farrar, S. Pelletier, J. Lugtenburg, J. Herzfeld, and R.G. Griffin. 1991. Mechanism of Proton Pumping in Bacteriorhodopsin by Solid-State NMR: The Protonation State of Tyrosine in the Light-Adapted and M States. Biochemistry. 30: 8366–8371.

19. Farrar, M.R., K. V. Lakshmi, S.O. Smith, R.S. Brown, J. Raap, J. Lugtenburg, R.G. Griffin, and J. Herzfeld. 1993. Solid state NMR study of [ε-^{13}C]Lys-bacteriorhodopsin: Schiff base photoisomerization. Biophys. J. 65: 310–315.

20. de Groot, H.J.M., S.O. Smith, J. Courtin, E. van den Berg, C. Winkel, J. Lugtenburg, R.G. Griffin, and J. Herzfeld. 1990. Solid-state ^{13}C and ^{15}N NMR study of the low pH forms of bacteriorhodopsin. Biochemistry. 29: 6873–6883.

21. Hu, J.G., B.Q. Sun, M. Bizounok, M.E. Hatcher, J.C. Lansing, J. Raap, P.J.E. Verdegem, J. Lugtenburg, R.G. Griffin, and J. Herzfeld. 1998. Early and late M intermediates in the bacteriorhodopsin photocycle: A solid-state NMR study. Biochemistry. 37: 8088–8096.

22. Petkova, A.T., M. Hatanaka, C.P. Jaroniec, J.G. Hu, M. Belenky, M. Verhoeven, J. Lugtenburg, R.G. Griffin, and J. Herzfeld. 2002. Tryptophan interactions in bacteriorhodopsin: A heteronuclear solid-state NMR study. Biochemistry. 41: 2429–2437.

23. Hu, J.G., B.Q. Sun, A.T. Petkova, R.G. Griffin, and J. Herzfeld. 1997. The predischarge chromophore in bacteriorhodopsin: A ^{15}N solid-state NMR study of the L photointermediate. Biochemistry. 36: 9316–9322.

24. Mak-Jurkauskas, M.L., V.S. Bajaj, M.K. Hornstein, M. Belenky, R.G. Griffin, and J. Herzfeld. 2008. Energy transformations early in the bacteriorhodopsin photocycle revealed by DNP-enhanced solid-state NMR. Proc. Natl. Acad. Sci. 105: 883–888.

25. Bajaj, V.S., M.L. Mak-Jurkauskas, M. Belenky, J. Herzfeld, and R.G. Griffin. 2009. Functional and shunt states of bacteriorhodopsin resolved by 250 GHz dynamic nuclear polarization-enhanced solid-state NMR. Proc. Natl. Acad. Sci. 106: 9244–9.

26. Becker-Baldus, J., C. Bamann, K. Saxena, H. Gustmann, L.J. Brown, R.C.D. Brown, C. Reiter, E. Bamberg, J. Wachtveitl, H. Schwalbe, and C. Glaubitz. 2015. Enlightening the photoactive site of channelrhodopsin-2 by DNP-enhanced solid-state NMR spectroscopy. Proc. Natl. Acad. Sci. 112: 9896–9901.

27. Kawamura, I., N. Kihara, M. Ohmine, K. Nishimura, S. Tuzi, H. Saitô, and A. Naito. 2007. Solid-state NMR studies of two backbone conformations at Tyr185 as a function of retinal configurations in the dark, light, and pressure adapted bacteriorhodopsins. J. Am. Chem. Soc. 129: 1016–1017.

28. Tomonaga, Y., T. Hidaka, I. Kawamura, T. Nishio, K. Ohsawa, T. Okitsu, A.

Wada, Y. Sudo, N. Kamo, A. Ramamoorthy, and A. Naito. 2011. An active photoreceptor intermediate revealed by in situ photoirradiated solid-state NMR spectroscopy. Biophys. J. 101: L50–L52.

29. Yomoda, H., Y. Makino, Y. Tomonaga, T. Hidaka, I. Kawamura, T. Okitsu, A. Wada, Y. Sudo, and A. Naito. 2014. Color-discriminating retinal configurations of sensory rhodopsin i by photo-irradiation solid-state NMR spectroscopy. Angew. Chemie Int. Ed. 53: 6960–6964.

30. Naito, A., and I. Kawamura. 2014. Photoactivated structural changes in photoreceptor membrane proteins as revealed by in situ photoirradiation solid-state NMR spectroscopy. In: Frances Separovic, A Naito, editors. Advances in Biological Solid-State NMR: Proteins and Membrane-Active Peptides. Cambridge, UK: Royal Society of Chemistry. pp. 387–404.

31. Naito, A., I. Kawamura, and N. Javkhlantugs. 2015. Recent solid-state NMR studies of membrane-bound peptides and proteins. Annu. Reports NMR Spectrosc. 86: 334–411.

32. Oshima, K., A. Shigeta, Y. Makino, I. Kawamura, T. Okitsu, A. Wada, S. Tuzi, T. Iwasa, and A. Naito. 2015. Characterization of photo-intermediates in the photo-reaction pathways of a bacteriorhodopsin Y185F mutant using in situ photo-irradiation solid-state NMR spectroscopy. Photochem. Photobiol. Sci. 14: 1694–1702.

33. Naito, A., Y. Makino, Y. Tasei, and I. Kawamura. 2018. Photoirradiatiion and microwave irradiation NMR spectroscopy. In: the Nuclear Magnetic Resonance Society of Japan, editor. Experimental Approaches of NMR Spectroscopy. Singapore: Springer. pp. 135–170.

34. Naito, A., Y. Makino, and I. Kawamura. 2017. In-Situ Photo Irradiation Solid-State NMR Spectroscopy Applied to Retinal-Binding Membrane Proteins. In: Graham A. Webb, editor. Modern Magnetic Resonance. Springer. pp. 1–22.

35. Kitajima-Ihara, T., Y. Furutani, D. Suzuki, K. Ihara, H. Kandori, M. Homma, and Y. Sudo. 2008. Salinibacter sensory rhodopsin: Sensory rhodopsin I-like protein from a eubacterium. J. Biol. Chem. 283: 23533–23541.

36. Kawamura, I., H. Yoshida, Y. Ikeda, S. Yamaguchi, S. Tuzi, H. Saitô, N. Kamo, and A. Naito. 2008. Dynamics change of phoborhodopsin and transducer by activation: Study Using D75N Mutant of the Receptor by Site-directed Solid-state ^{13}C NMR. Photochem. Photobiol. 84: 921–930.

37. Sudo, Y., M. Yamabi, M. Iwamoto, K. Shimono, and N. Kamo. 2003. Interaction of Natronobacterium pharaonis phoborhodopsin (sensory rhodopsin II) with its cognate transducer probed by increase in the thermal stability. Photochem. Photobiol. 78: 511–6.

38. F. London. 1937. Théorie quantique des courants interatomiques dans les combinaisons aromatiques. J. Phys. Le Radium. 8: 397–409.

39. R. Ditchfield. 1972. Molecular Orbital Theory of Magnetic Shielding and Magnetic Susceptibility. J. Chem. Phys. 56: 5688.

40. Ditchfield, R. 1974. Self-consistent perturbation theory of diamagnetism I. A gauge-invariant LCAO method for N.M.R. Chemical shifts. Mol. Phys. 27: 789–807.

41. Woliński, K., and A.J. Sadlej. 1980. Self-consistent perturbation theory open-shell states in perturbation-dependent non-orthogonal basis sets. Mol. Phys. 41: 1419–1430.

42. Wolinski, K., J.F. Hinton, and P. Pulay. 1990. Efficient Implementation of the Gauge-Independent Atomic Orbital Method for NMR Chemical Shift Calculations. J. Am. Chem. Soc. 112: 8251–8260.

43. Frisch, M.J., G.W. Trucks, H.B. Schlegel, G.E. Scuseria, M.A. Robb, J.R. Cheeseman, J.A. Montgomery, T.V. Jr., K.N. Kudin, J.C. Burant, J.M. Millam, S.S. Iyengar, J. Tomasi, V. Barone, B. Mennucci, M. Cossi, G. Scalmani, N. Rega, G.A. Petersson, H. Nakatsuji, M. Hada, M. Ehara, K. Toyota, R. Fukuda, J. Hasegawa, M. Ishida, T. Nakajima, Y. Honda, O. Kitao, H. Nakai, M. Klene, X. Li, J.E. Knox, H.P. Hratchian, J.B. Cross, V. Bakken, C. Adamo, J. Jaramillo, R. Gomperts, R.E. Stratmann, O. Yazyev, A.J. Austin, R. Cammi, C. Pomelli, J.W. Ochterski, P.Y. Ayala, K. Morokuma, G.A. Voth, P. Salvador, J.J. Dannenberg, V.G. Zakrzewski, S. Dapprich, A.D. Daniels, M.C. Strain, O. Farkas, D.K. Malick, A.D. Rabuck, K. Raghavachari, J.B. Foresman, J. V. Ortiz, Q. Cui, A.G. Baboul, S. Clifford, J. Cioslowski, B.B. Stefanov, G. Liu, A. Liashenko, P. Piskorz, I. Komaromi, R.L. Martin, D.J. Fox, T. Keith, M.A. Al-Laham, C.Y. Peng, A. Nanayakkara, M. Challacombe, P.M.W. Gill, B. Johnson, W. Chen, M.W. Wong, C. Gonzalez, J.A. Pople, and 2004. Gaussian, Inc., Wallingford CT. 2004. Gaussian 09, Revision A.02. .

44. Luecke, H., B. Schobert, J.K. Lanyi, E.N. Spudich, and J.L. Spudich. 2016. Crystal Structure of Sensory Rhodopsin II at 2.4 Angstroms: Insights into Color Tuning and Transducer Interaction. 293: 1499–1503.

45. Tateishi, Y., T. Abe, J. Tamogami, Y. Nakao, T. Kikukawa, N. Kamo, and M. Unno. 2011. Spectroscopic evidence for the formation of an N intermediate during the photocycle of sensory rhodopsin II (phoborhodopsin) from

natronobacterium pharaonis. Biochemistry. 50: 2135–2143.

46. Roy, S., T. Kikukawa, P. Sharma, and N. Kamo. 2006. All-optical switching in Pharaonis phoborhodopsin protein molecules. IEEE Trans Nanobioscience. 5: 178–87.

47. Lakshmi, K. V., M.R. Farrar, J. Herzfeld, R.G. Griffin, J. Raap, J. Lugtenburg, and R.G. Griffin. 1994. Solid State^{13}C and^{15}N NMR Investigations of the N Intermediate of Bacteriorhodopsin. Biochemistry. 33: 8853–8857.

48. Touw, S.I.E., H.J.M. De Groot, and F. Buda. 2004. DFT calculations of the^{1}H chemical shifts and^{13}C chemical shift tensors of retinal isomers. J. Mol. Struct. THEOCHEM. 711: 141–147.

49. Harbison, G.S., S.O. Smith, J.A. Pardoen, C. Winkel, J. Lugtenburg, J. Herzfeld, R. Mathies, and R.G. Griffin. 1984. Dark-adapted bacteriorhodopsin contains 13-cis, 15-syn and all-trans, 15-anti retinal Schiff bases. Proc. Natl. Acad. Sci. 81: 1706–1709.